

pubs.acs.org/JPCB Article

# **Contribution of Signaling Partner Association to Strigolactone Receptor Selectivity**

Jiming Chen, Tanner J. Dean, and Diwakar Shukla\*



Cite This: J. Phys. Chem. B 2024, 128, 698-705



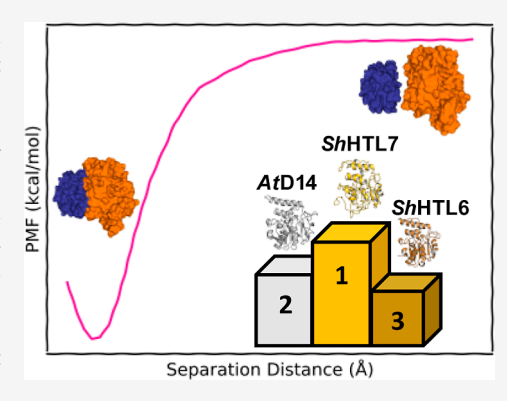
**ACCESS** I

III Metrics & More

Article Recommendations

Supporting Information

**ABSTRACT:** The parasitic plant witchweed, *Striga hermonthica*, results in agricultural losses of billions of dollars per year. It perceives its host via plant hormones called strigolactones, which act as germination stimulants for witchweed. Strigolactone signaling involves substrate binding to the strigolactone receptor, followed by substrate hydrolysis and a conformational change from an inactive, or open state, to an active, or closed state. In the active state, the receptor associates with a signaling partner, MAX2. Recently, it was shown that this MAX2 association process acts as a strong contributor to the uniquely high signaling activity observed in *ShHTL7*; however, it is unknown why *ShHTL7* has enhanced MAX2 association affinity. Using an umbrella sampling molecular dynamics approach, we characterized the association processes of *AtD14*, *ShHTL7*, a mutant of *ShHTL7*, and *ShHTL6* with MAX2 homologue *OsD3*. From these results, we show that *ShHTL7* has an enhanced standard binding free energy of *OsD3* compared to those



of the other receptors. Additionally, our results suggest that the overall topology of the T2/T3 helix region is likely an important modulator of MAX2 binding. Thus, differences in MAX2 association, modulated by differences in the T2/T3 helix region, are a contributor to differences in signaling activity between different strigolactone receptors.

#### **■ INTRODUCTION**

Strigolactones are a class of endogenous plant hormones involved in the regulation of shoot branching, hypocotyl elongation, and root architecture in plants. 1-3 Signal transduction begins with the binding of strigolactone to its receptor, DWARF14 (D14). This receptor also functions as a hydrolase enzyme for the hormone, and after the substrate binds, it is hydrolyzed by the receptor.<sup>4,5</sup> This hydrolysis reaction covalently modifies the receptor, promoting a conformational change of the receptor to its closed or active state which associates with MAX2 and SMXL proteins. 4,6,7 This signaling complex is ubiquitinated and degraded, inducing a signaling response.4-8 It has also been shown that MAX2 can interact with inactive-state D14 via its C-terminal helix and inhibit substrate hydrolysis<sup>6</sup> and that conformational dynamics of MAX2 plays a role in transducing the strigolactone signal. Despite high sequence, structure, and binding pocket conservation across different strigolactone receptors (SL receptors), a receptor found in the parasitic plant Striga, ShHTL7, has been observed to display a picomolar EC50 toward strigolactone when measured via a germination response assay. This high sensitivity has previously been attributed to the binding pocket volume of ShHTL7, 10-12 however, this does not account for the effects of the subsequent transformations leading to the formation of the signaling complex: substrate hydrolysis, activation, and association with MAX2.

Recently, Wang et al. found that measured binding affinities for naturally occurring strigolactone are similar across different HTL proteins found in Striga. However, ShHTL7 had a higher affinity for MAX2 compared to other HTL proteins when evaluated with an in vitro pull-down assay. 13 This similarity in ligand affinity suggests that the binding and hydrolysis activity are similar across HTL proteins; thus, the difference in MAX2 affinity of ShHTL7 is likely due to either a higher likelihood of being in an active conformation or a stronger interaction with MAX2 while in the active conformation. Additionally, this study found that mutating five key residues on ShHTL6 to their equivalent ShHTL7 residues promoted association of the mutant ShHTL6 over the wild type. <sup>13</sup> In our previous work, we determined that while ShHTL7 has a lower propensity for apo activation compared to AtD14, the enhancement of activation is 50 times greater, indicating that the presence of a substrate greatly enhances its likelihood of being in the active state that allows it to form a signaling complex with MAX2.14,15 Since there is a ~10000-fold difference in signaling activity between ShHTL7 and other receptors, the difference in activation

Received: October 19, 2023
Revised: December 11, 2023
Accepted: December 19, 2023
Published: January 9, 2024





enhancement by covalent modification does not completely account for the difference. Here, we aim to evaluate the contribution of D14/HTL-MAX2 binding to the high signaling activity of *Sh*HTL7 by computing the standard binding free energies of association between several SL receptors and the rice homologue of MAX2, *Os*D3.

Since decoupling of the effects of activation and MAX2 affinity on the formation of the SL receptor-MAX2 complex is difficult in vitro, we apply molecular dynamics (MD) simulations to characterize the association pathways of active-state AtD14, ShHTL7, a mutant of ShHTL7 with five residues mutated to their equivalent ShHTL6 residues, and ShHTL6 with OsD3, the Oryza sativa homologue of AtMAX2. For the ShHTL7 mutant, we mutated the five residues that were shown to produce ShHTL7-like association properties in ShHTL6.<sup>13</sup> The structure of AtD14 in complex with OsD3 is shown in Figure 1a, and the mutation sites in wild ShHTL7

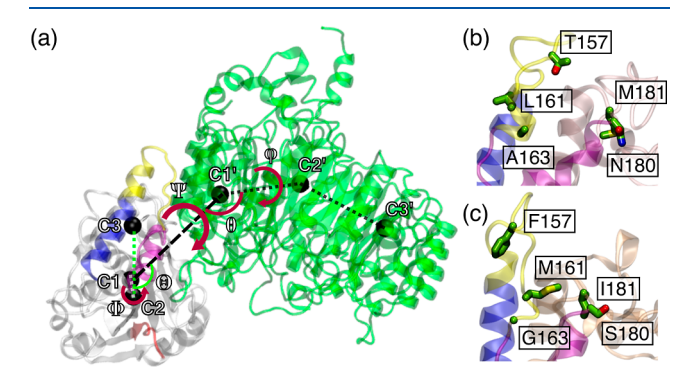


**Figure 1.** (a) Complex of AtD14 and OsD3. The T1, T2, and T3 helices of AtD14 are shown in blue, yellow, and purple, respectively, and the D-loop of AtD14 is shown in red. OsMAX2 is shown in green. Centers of mass of the C1, C2, C3, C1′, C2′, and C3′ residue groups are depicted with black spheres. Restrained collective variables are defined as follows: r (separation distance): C1–C1′ distance, Θ: C1′–C1–C2 angle,  $\theta$ : C1–C1′-C2′,  $\Phi$ : C1′–C1–C2–C3 dihedral,  $\phi$ : C1–C1′-C2′-C3′ dihedral,  $\Psi$ : C2–C1–C1′-C2′ dihedral. Residue groups were defined as C1:2–263; C2:1–120, 195–263; C3:134–194; C1′: 854–965; C2′: 266–443; C3′: 560–700 using AtD14 numbering, with sequence-equivalent regions selected for ShHTL complexes. (b) Residues mutated to ShHTL6 in wild-type ShHTL7 and (c) residues mutated to ShHTL7 mutant.

and their equivalent ShHTL6 residues in the ShHTL7 mutant are shown in Figure 1b,c, respectively. Using an umbrella sampling procedure developed by Gumbart et al., 16,17 we computed the standard association free energies of each D14/ HTL receptor with OsD3. Umbrella sampling provides an efficient method of calculating a free energy profile along a particular pathway by running a series of harmonically restrained simulations at short intervals along the path.1 The potential of mean force (PMF) along the pathway is then recovered using unbiasing methods such as the weighted histogram analysis method<sup>19</sup> and the multistate Bennett acceptance ratio method (MBAR).<sup>20</sup> Umbrella sampling provides an advantage over traditional long MD, particularly for large systems such as protein-protein complexes, because the presence of restraints along the pathway allows for sampling of a full transition that may be inaccessible to unbiased MD simulations due to time scale constraints. This method has previously been applied to compute association of other plant hormone signaling complexes. 21,22 Using this procedure, we determined that the standard binding free energy of wild-type ShHTL7 is greater in magnitude than those of AtD14, mutant ShHTL7, and ShHTL6, indicating that this association process contributes to the difference in ShHTL7 sensitivity in addition to activation. Additionally, we find that the high affinity of ShHTL7 for MAX2 is largely driven by significant stabilization of the lid domain upon association, rather than by specific interfacial interactions that are stronger in the ShHTL7-OsD3 complex.

# RESULTS

Separation Potentials of Mean Force Similar for AtD14, ShHTL7, and ShHTL6 Complexes. To evaluate the association free energies of AtD14, ShHTL7, ShHTL7 mutant, and ShHTL6 with D3, we first applied umbrella sampling simulations to compute the PMFs of separation. The separation PMFs for AtD14, ShHTL7 wild type, and ShHTL6 all had a similar depth of  $\sim$ 63 kcal/mol (Figure 2). The ShHTL7 mutant had a more shallow PMF depth of  $\sim$ 55 kcal/mol. These PMF depths initially appear to contradict the experimental results that show that ShHTL7 has a greater affinity for MAX2. However, it is important to note that these PMF values were computed with restraints placed on the relative orientation and RMSDs of the proteins. Since the free

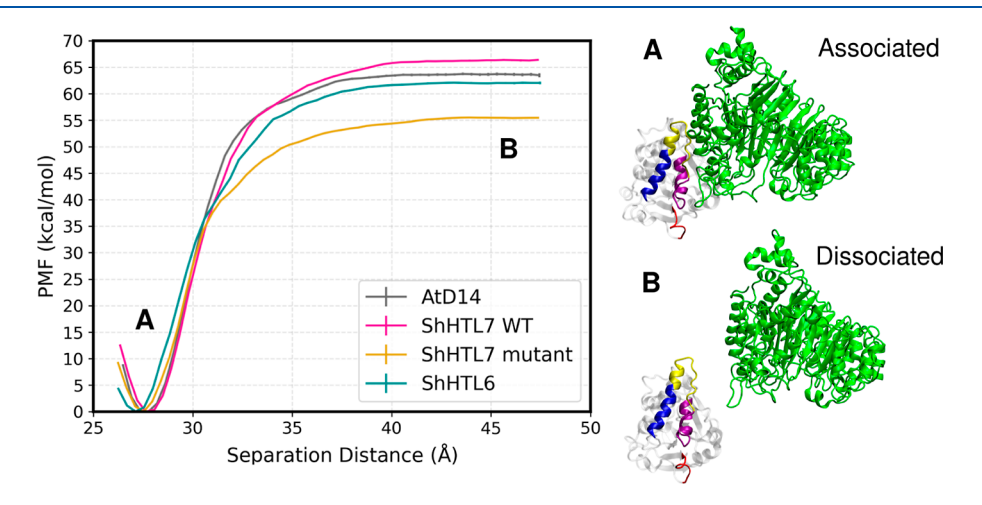


Figure 2. Separation potentials of mean force for AtD14, ShHTL7 wild type, ShHTL7 mutant, and ShHTL6 with OsD3. The associated and dissociated states of AtD14 are shown and labeled A and B, respectively.

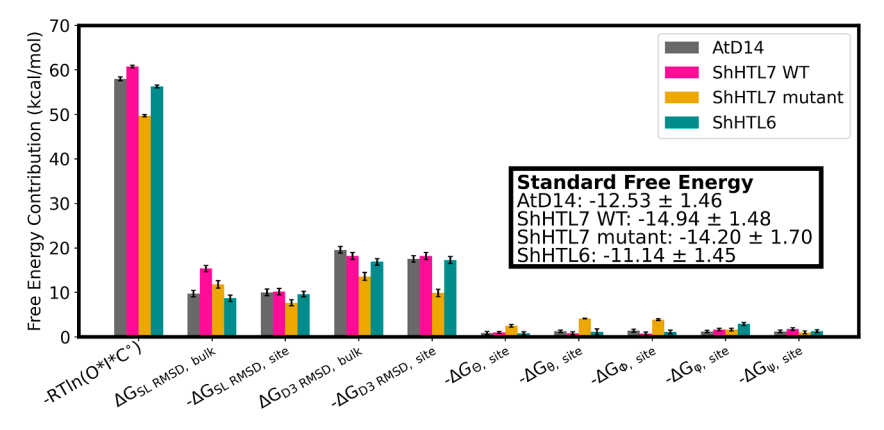
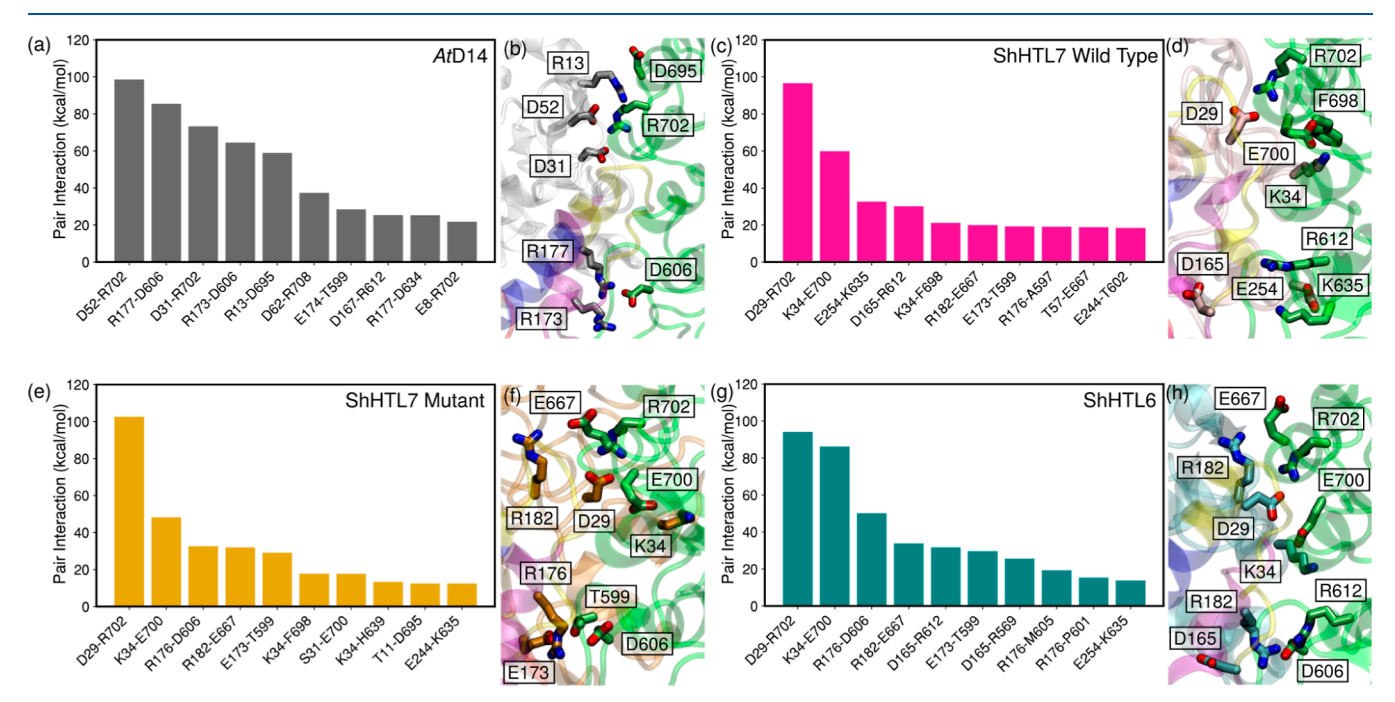


Figure 3. Contributions of separation  $[-RT \ln(O \times I \times C^{\circ})]$ , RMSD restraint terms, and angular restraint terms to the overall binding free energy. For RMSD restraint terms, "bulk" refers to the D14/HTL-D3 dissociated state, and "site" refers to the D14/HTL-D3 associated state.



**Figure 4.** Top pairwise residue interactions for (a,b) AtD14, (c,d) ShHTL7 wild type, (e,f) ShHTL7 mutant, and (g,h) ShHTL6. Residue pairs with the top 10 strongest attractive interactions for each protein are shown in (a,c,e,g), and residues involved in the top 5 interactions are shown in (b,d,f,h).

energy associated with removing these restraints may be different for each protein complex, we computed the standard association free energies of each complex by correcting for the applied restraints using the method in Gumbart et al. <sup>16,17</sup>

ShHTL7 Has the Most Favorable Association with OsD3 after Restraint Contributions. To compute the standard free energies of association, we performed additional umbrella sampling along all RMSD restraints and angular restraints in the associated ("site") state. Performing additional simulations for the bulk state was unnecessary since their free energy contributions were able to be calculated analytically as detailed in the Supporting Information section on calculation of standard binding free energy. Free energy contributions of removing RMSD restraints and associated-state angular restraints are shown in Figure 3, and the exact values are shown in Table S1. For the ShHTL6 and both ShHTL7 complexes, these values are qualitatively in agreement with the findings of Wang et al. in that ShHTL7 has a higher association affinity for MAX2 than ShHTL6.<sup>13</sup> Additionally, Wang et al.

found that mutation of five key lid helix residues on ShHTL6 to equivalent ShHTL7 residues enhanced association affinity, 13 and we show that mutation of the five residues to equivalent ShHTL6 residues lowers association affinity. The  $\Delta\Delta G$  values of ShHTL6, ShHTL7 mutant, and AtD14 vs ShHTL7 are all positive, demonstrating the higher association of ShHTL7 to OsD3 (Figure S4). We expect the standard binding free energy of the ShHTL7 mutant to decrease from ShHTL7 due to the five key lid helix residue mutations, and indeed, the standard binding free energy value is reduced from -14.94 to -14.20 kcal/mol. The decreased value of the ShHTL7 mutant may be explained by the mutation of five residues at the T2 helix. While the differences between bulk and site  $\Delta G_{\text{D3 RMSD}}$  show low variation across protein complexes in Figure 3,  $\Delta G_{\rm SL, RMSD}$ varies more between complexes and is an important driving force responsible for the differences in the standard association free energies. For further investigation of the drivers of the differences in standard association free energy, we evaluated

the contributions of top interacting interfacial residue pairs as well as the dynamics of the SL receptors.

Top Interacting Contacts Show Similar Pair Interaction Energies across SL Receptor-D3 Complexes. To determine the key interacting residue pairs that promote receptor-D3 association, we employed pair interaction calculations in the gRINN package.<sup>23</sup> Briefly, this entailed identifying a set of frequently contacting residues on the interface between the SL receptor and OsD3 and computing the average potential energy of each pair interaction over the length of the simulation trajectories. Pair interaction energies of the interfacial residue pairs with the top ten highest interaction energies are shown in Figure 4a,c,e,g. Residues involved in the top five pairs with the highest interaction energies are shown in Figure 4b,d,f,h. Simulation trajectories from bound umbrella sampling windows were used for this calculation. For all four complexes, the top pair was the R702 residue on OsD3 forming a salt bridge with an aspartate residue on the SL receptor, D52 on AtD14, and D29 on ShHTL7 and ShHTL6. For all of the ShHTL-OsD3 complexes, the next strongest pair interaction was K34-E700. The pair interaction value for a pair of residues varied from ~50 to ~80 kcal/mol, indicating that while this interaction remains a key driver of association in the different HTL receptors, the relative positioning of these interfacial residues differs slightly between complexes. Notably, the magnitudes of the highest pair interaction energies of interacting residues are similar across the four protein complexes. This indicates that the differences in standard association free energy are driven by factors other than specific interfacial interactions. Since the contributions of the various restraint terms to association free energy showed that SL receptor RMSD is a strong modulator of the free energy differences, we investigated the flexibility of various regions on SL receptors in their OsD3 bound and unbound states.

Loss of T2/T3 Region Disorder upon D3 Binding Most **Prevalent in ShHTL7.** To evaluate why the SL receptor RMSD terms differed among the various systems, we computed crystallographic B-factors from simulations in the bound and unbound states for each complex, shown in Figure 5. For all systems, there is a region of high *B*-factor indicating greater flexibility in the T2/T3 helix region of the lid domain. Notably, the *B*-factor of this region in *Sh*HTL7 is the highest of all systems in the bulk (dissociated) phase and decreases significantly in the site (associated) phase, from  $\sim$ 300 to  $\sim$ 20 Å<sup>2</sup>. This indicates that association with D3 stabilizes the T2 helix of wild-type ShHTL7 to a greater extent than the other receptors considered. In AtD14, the B-factor of the T2 helix also decreases upon D3 binding, however, the T2 helix shows a considerably lower *B*-factor in the unbound state ( $\sim 100 \text{ Å}^2$ ) compared to that seen in ShHTL7. This indicates that the stabilization of the T2 helix provides less contribution to the overall free energy of association, which is consistent with the lower calculated contribution of the receptor RMSD term. The ShHTL7 mutant, similarly to wild-type ShHTL7, shows high flexibility in the T2 region, however, the B-factors of this region remain high ( $\sim$ 100–150 Å<sup>2</sup>) upon association with D3, indicating that D3 association provides less stabilization of this region in mutant ShHTL7 than in wild-type ShHTL7. Finally, ShHTL6 displays a lower B-factor in the T2 helix region than either wild-type or mutant ShHTL7 in the unbound state. The T2/T3 loop in ShHTL6 shows a significant decrease in the Bfactor upon D3 binding. This is also observed in wild-type

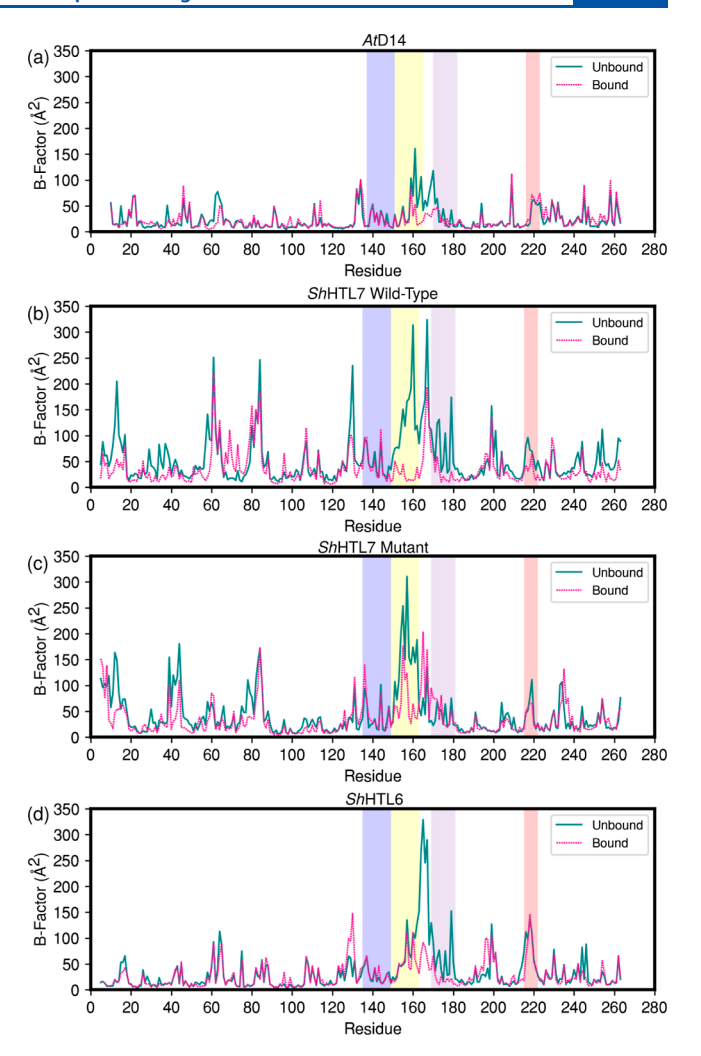


**Figure 5.** *B*-factors calculated in the D3-bound and unbound states for (a) *At*D14, (b) *Sh*HTL7 wild type, (c) *Sh*HTL7 mutant, and (d) *Sh*HTL6. The T1, T2, and T3 helices are colored blue, yellow, and purple, respectively. The D-loop is highlighted in red.

ShHTL7, and thus, it is unlikely that this region is a key factor for the high overall association free energy observed in ShHTL7.

In all four SL receptor-D3 complexes, the unfolded portion of the T2 helix and the loop between the T2 and T3 helices form a predominantly hydrophobic interface with D3, as shown in Figure 6. Hydrophobic patches at protein-protein interfaces have previously been shown to function as important recognition sites for various protein-protein interactions. 24-27 A sequence alignment of AtD14, ShHTL7, and ShHTL6 shows a high degree of hydrophobicity in the portion of the T2 helix that is unfolded in the active state, along with a portion of the loop between the T2 and T3 helices (Figure S1). Specifically, the region from G158/156 on the helix to D167/165 on the T2/T3 loop is entirely composed of hydrophobic residues, with the exception of T157 on wild-type ShHTL7. The conservation of this hydrophobicity suggests that the unfolded portion of the T2 helix may function as a key recognition site for association with MAX2/D3.

#### DISCUSSION

Using an umbrella sampling procedure, we computed the standard association free energies of AtD14, wild-type

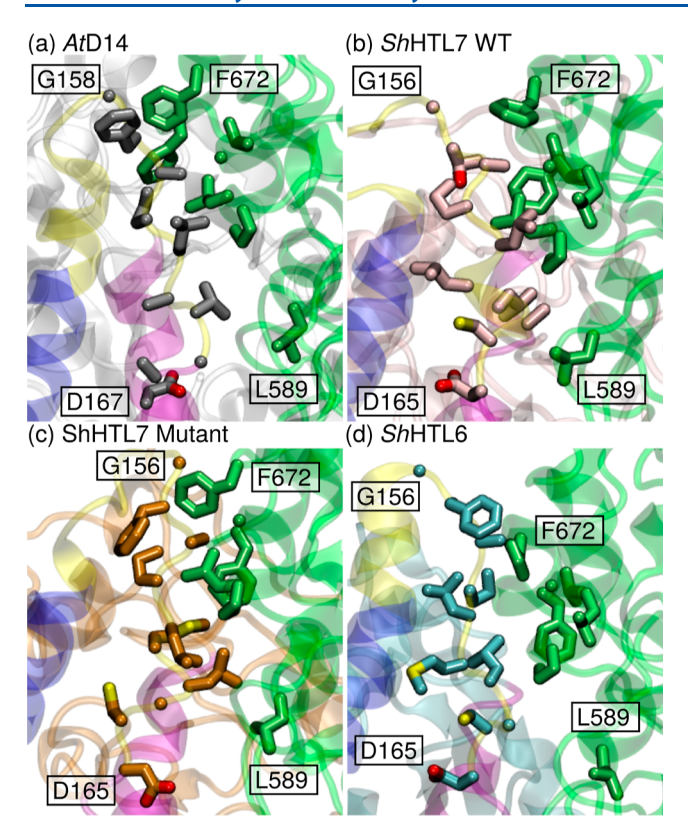


**Figure 6.** Predominantly hydrophobic interface between *Os*D3 and the unfolded T2 helix of (a) *At*D14, (b) *Sh*HTL7 wild type, (c) *Sh*HTL7 mutant, and (d) *Sh*HTL6. The T1, T2, and T3 helices of the SL receptors are shown in blue, yellow, and purple, respectively, and *Os*D3 is shown in green.

ShHTL7, mutant ShHTL7, and ShHTL6 with OsMAX2. By evaluating the contributions of various restraint terms to the overall association free energy, we have determined that differences in stabilization of the T2 helix region upon association are key to determining selectivity in OsD3 binding between the different receptors. Additionally, strengths of top residue pair interactions are similar across the four protein complexes, which further suggests that selectivity in association is driven by the overall flexibility of the receptors, particularly in the T2/T3 helix region, rather than specific interactions with OsD3. Since the interfacial residues with the highest pair interaction energies are similar across the four systems evaluated and are close in pair interaction energy, our results suggest that the selectivity is modulated by conformational dynamics of the complex, specifically the T2 helix region, rather than specific interactions at the interface. This is corroborated by the magnitude of SL receptor RMSD restraint terms during the standard binding free energy calculation. It is also corroborated by the B-factors of the four different SL receptors showing differences in T2 helix flexibility in unbound and bound states across the four receptors.

The higher association of *Os*D3 with *Sh*HTL7 compared to the other receptors is consistent with the results of Wang et al. showing that *Sh*HTL7 shows more binding activity toward *At*MAX2 compared to other *Sh*HTL proteins. <sup>13</sup> Additionally, loss of *Os*D3 association affinity when five residues in the T2/T3 helix region of *Sh*HTL7 (T157, L161, A163, N180, and M181) were mutated to their equivalent *Sh*HTL6 residues (F157, M161, G163, I181, and S180) suggests that this region is important for the association process. This is also consistent

with the result from Wang et al. that mutation of these five residues in ShHTL6 to the equivalent ShHTL7 residues enhanced association with AtMAX2.13 Notably, all of these mutations are to residues with similar chemical properties, i.e., polar to polar or hydrophobic to hydrophobic, with the exception of T157 ShHTL7 and F157 in ShHTL6. While this in principle could suggest that T157 in ShHTL7 forms an additional hydrogen bonding interaction with MAX2 that is not present when a phenylalanine is present at the same position, this is not supported by our residue pair interaction strength calculations showing T157 is not involved in any of the strongest residue pair interactions at the interface. However, T157 in ShHTL7 is the only polar residue between G156 (ShHTLs)/G158 (AtD14) and D165 (ShHTLs)/D167 (AtD14), suggesting that it may play a role in optimizing the geometry of the region for MAX2/D3 recognition. Additionally, it is also possible that this region modulates an induced fit mechanism of binding in which a conformational change is coupled with association. This has been observed in other protein systems with disordered regions.  $^{28-30}$  Several previous studies have identified this T157 residue as an important modulator of substrate binding in *Sh*HTL7. <sup>31–34</sup> Our analysis suggests that in addition to enhancing substrate binding, this residue could play a role in enhancing signaling partner association by modulating the geometry of the T2/T3 region of the receptor. The idea that the T2/T3 region in strigolactone is a key MAX2/D3 recognition region is additionally supported by the observations that although standard association free energies differ between systems, the top pair interaction energies are fairly consistent and the RMSD of this region is a large contributor to differences in association free energy between the complexes studied.

In our previous work, we determined that ShHTL7 has several advantages in substrate recognition and receptor activation that likely contribute to its high strigolactone sensitivity. Here, we show that the signaling partner association also contributes to the high signaling ability of ShHTL7. This indicates that the high MAX2 binding affinity and subsequent high sensitivity of ShHTL7 is not the result of any single step in the strigolactone perception pathway on its own but rather the combined effects of all steps. This idea also has implications in the design of small-molecule modulators to control witchweed by targeting this signaling pathway. Previous methods that have been proposed include direct inhibition of SL receptors<sup>35,36</sup> and induction of suicidal germination using strigolactone mimics. 33,37,38 Based on the finding that MAX2 association is an important contributor to the high signaling ability of ShHTL7, another possible strategy is the inhibition of MAX2 association. Small-molecule inhibitors of protein-protein interactions have been studied in the context of drug discovery. <sup>39,40</sup> Given that differences in the T2/T3 helix region may be key drivers of selectivity in MAX2 association, small molecules that bind to this region could be a potent and selective inhibitor of witchweed germination.

# METHODS

**System Preparation.** The associated structure of *At*D14 and *Os*D3 was obtained from PDB code 5HZG.<sup>4</sup> Active state structures for other systems were constructed by homology model using Modeler.<sup>41–43</sup> Each complex was solvated in a TIP3P water box with a 0.15 M NaCl concentration. The AMBER ff14SB force field was used for proteins. Each system

was minimized using a conjugate gradient descent method followed by heating to 0 to 300 K and 5 ns equilibration. The temperature was maintained at 300 K using the Langevin thermostat, <sup>44</sup> and pressure was maintained at 1.0 bar using the Langevin barostat. <sup>45</sup> Bonds to hydrogen were constrained by using the SHAKE algorithm. Long-range electrostatics were computed using the particle mesh Ewald algorithm. <sup>46</sup> All production runs were performed using NAMD 2.14. <sup>47</sup>

**Umbrella Sampling Protocol.** A restrained umbrella sampling procedure was used to generate the separation PMFs. Harmonic restraints were placed on five orientational angles (shown in Figure 1) and RMSDs of both proteins in each system, as described in Gumbart et al. <sup>16,17</sup> The average values of each orientational restraint over a 1 ns unbiased simulation were used to determine centers of orientational restraints. Restraint centers and force constants for each system are listed in Table S2. After the equilibration, initial structures for the umbrella sampling procedure were generated using a steered MD simulation with orientation and RMSD restraints applied. Window centers were set at 0.33 Å intervals. In total, 64 windows with centers ranging from 26 to 46 Å C1–C1' separation distance were used for the umbrella sampling procedure. Simulation time per umbrella sampling window for each protein complex is provided in Tables S3–S6.

To compute the free energy contributions of the orientation and RMSD restraints when the overall association free energies were calculated, further umbrella sampling simulations were performed on each restraint. Initial structures for these simulations were obtained from adaptive biasing force (ABF) simulations. 48,49 ABF simulations were initiated from bound umbrella sampling windows, defined as windows closest to the minimum value of the separation PMF, and were performed along both RMSD and all orientational restraints. In addition, ABF simulations were also initiated from unbound umbrella sampling windows to obtain structures to calculate the PMF of removing the RMSD restraints from the unbound state. PMFs of these additional umbrella sampling simulations are shown in Figures S2-S3. Free energy contributions of angular and orientational restraints were calculated analytically; thus, no additional simulations were performed for these restraints. All PMFs and uncertainties were calculated from umbrella sampling simulations using the MBAR method, implemented in pyMBAR.<sup>20</sup>

**Free Energy Calculations.** Overall free energies were calculated using

$$\Delta G_{\text{binding}} = -RT \ln(K_{\text{A}} C^{\circ}) \tag{1}$$

where  $C^{\circ}$  is a standard concentration value of 1/1661 Å<sup>3</sup>.  $K_{\rm A}$  was calculated by using an integral of the separation PMF with corrections obtained from ensemble averages of orientation and RMSD restraints. Full details for this procedure are provided in the Supporting Information, calculation of standard binding free energy.

**Pair Interaction Calculations.** Pair interaction energies were computed using the pair interaction interface in NAMD 2.14. Calculations were performed on all bound-state trajectories, defined as umbrella sampling windows of 5–7 for all complexes. First, a set of frequently interacting pairs were identified by calculating pairwise distances between SL receptor and D3 residues at the binding interface and selecting all pairs within a cutoff inter-residue distance of 12 Å. The average of the pair interaction energy for each pair across all

simulation frames in bound windows was subsequently calculated.

**B-Factor Calculations.** To compute *B*-factors, root-mean-square fluctuation (RMSF) was first calculated using the CPPTRAJ software. So *B*-factors were computed using the formula

$$B = \frac{8}{3}\pi^2 (RMSF)^2 \tag{2}$$

# ASSOCIATED CONTENT

# Supporting Information

The Supporting Information is available free of charge at https://pubs.acs.org/doi/10.1021/acs.jpcb.3c06940.

Term contributions to the overall association free energies, protein sequence alignment, restraints used, total sampling for each system, PMFs of all restraints, standard association free energy comparisons, and calculation of standard binding free energies (PDF)

#### AUTHOR INFORMATION

#### **Corresponding Author**

Diwakar Shukla — Department of Chemical and Biomolecular Engineering, University of Illinois at Urbana—Champaign, Urbana, Illinois 61801, United States; Center for Biophysics and Quantitative Biology, Department of Bioengineering, and Department of Plant Biology, University of Illinois at Urbana—Champaign, Urbana, Illinois 61801, United States; orcid.org/0000-0003-4079-5381; Email: diwakar@illinois.edu

#### **Authors**

Jiming Chen – Department of Chemical and Biomolecular Engineering, University of Illinois at Urbana–Champaign, Urbana, Illinois 61801, United States

Tanner J. Dean — Center for Biophysics and Quantitative Biology, University of Illinois at Urbana—Champaign, Urbana, Illinois 61801, United States; orcid.org/0000-0002-3423-4177

Complete contact information is available at: https://pubs.acs.org/10.1021/acs.jpcb.3c06940

# Notes

The authors declare no competing financial interest.

# ACKNOWLEDGMENTS

This research was part of the Blue Waters sustained-petascale computing project, which was supported by the National Science Foundation (award nos. OCI-0725070 and ACI-1238993), the State of Illinois, and, as of December 2019, the National Geospatial-Intelligence Agency. Blue Waters was a joint effort of the University of Illinois at Urbana—Champaign and its National Center for Supercomputing Applications. T.D. and D.S. acknowledge support from the Molecule Maker Lab Institute (NSF CHE 2019897). J.C. is a member of the NIH Chemistry-Biology Interface Training Program (T32-GM136629). D.S. acknowledges support from the CAS Fellowship, Center for Advanced Studies at the University of Illinois at Urbana—Champaign, and a Sloan Research Fellowship from the Alfred P. Sloan Foundation.

#### REFERENCES

- (1) Umehara, M.; Hanada, A.; Yoshida, S.; Akiyama, K.; Arite, T.; Takeda-Kamiya, N.; Magome, H.; Kamiya, Y.; Shirasu, K.; Yoneyama, K.; Kyozuka, J.; Yamaguchi, S. Inhibition of shoot branching by new terpenoid plant hormones. *Nature* **2008**, *455*, 195–200.
- (2) Gomez-Roldan, V.; Fermas, S.; Brewer, P. B.; Puech-Pagès, V.; Dun, E. A.; Pillot, J.-P.; Letisse, F.; Matusova, R.; Danoun, S.; Portais, J.-C.; Bouwmeester, H.; Bécard, G.; Beveridge, C. A.; Rameau, C.; Rochange, S. F. Strigolactone inhibition of shoot branching. *Nature* **2008**, *455*, 189–194.
- (3) Waters, M. T.; Gutjahr, C.; Bennett, T.; Nelson, D. C. Strigolactone Signaling and Evolution. *Annu. Rev. Plant Biol.* **2017**, *68*, 291–322.
- (4) Yao, R.; Ming, Z.; Yan, L.; Li, S.; Wang, F.; Ma, S.; Yu, C.; Yang, M.; Chen, L.; Chen, L.; et al. DWARF14 is a non-canonical hormone receptor for strigolactone. *Nature* **2016**, *536*, 469–473.
- (5) de Saint Germain, A.; Clavé, G.; Badet-Denisot, M.-A.; Pillot, J.-P.; Cornu, D.; Le Caer, J. P.; Burger, M.; Pelissier, F.; Retailleau, P.; Turnbull, C.; Bonhomme, S.; Chory, J.; Rameau, C.; Boyer, F.-D. An histidine covalent receptor and butenolide complex mediates strigolactone perception. *Nat. Chem. Biol.* **2016**, *12*, 787–794.
- (6) Shabek, N.; Ticchiarelli, F.; Mao, H.; Hinds, T. R.; Leyser, O.; Zheng, N. Structural plasticity of D3–D14 ubiquitin ligase in strigolactone signalling. *Nature* **2018**, *563*, 652–656.
- (7) Tal, L.; Palayam, M.; Ron, M.; Young, A.; Britt, A.; Shabek, N. A conformational switch in the SCF-D3/MAX2 ubiquitin ligase facilitates strigolactone signalling. *Nat. Plants* **2022**, *8*, 561–573.
- (8) Bürger, M.; Chory, J. The Many Models of Strigolactone Signaling. *Trends Plant Sci.* **2020**, *25*, 395–405.
- (9) Toh, S.; Holbrook-Smith, D.; Stogios, P. J.; Onopriyenko, O.; Lumba, S.; Tsuchiya, Y.; Savchenko, A.; McCourt, P. Structure-function analysis identifies highly sensitive strigolactone receptors in Striga. *Science* **2015**, 350, 203–207.
- (10) Conn, C. E.; Bythell-Douglas, R.; Neumann, D.; Yoshida, S.; Whittington, B.; Westwood, J. H.; Shirasu, K.; Bond, C. S.; Dyer, K. A.; Nelson, D. C. Convergent evolution of strigolactone perception enabled host detection in parasitic plants. *Science* **2015**, 349, 540–543.
- (11) Xu, Y.; Miyakawa, T.; Nakamura, H.; Nakamura, A.; Imamura, Y.; Asami, T.; Tanokura, M. Structural basis of unique ligand specificity of KAI2-like protein from parasitic weed Striga hermonthica. *Sci. Rep.* **2016**, *6*, 31386.
- (12) Xu, Y.; Miyakawa, T.; Nosaki, S.; Nakamura, A.; Lyu, Y.; Nakamura, H.; Ohto, U.; Ishida, H.; Shimizu, T.; Asami, T.; Tanokura, M. Structural analysis of HTL and D14 proteins reveals the basis for ligand selectivity in Striga. *Nat. Commun.* **2018**, *9*, 3947.
- (13) Wang, Y.; Yao, R.; Du, X.; Guo, L.; Chen, L.; Xie, D.; Smith, S. M. Molecular basis for high ligand sensitivity and selectivity of strigolactone receptors in Striga. *Plant Physiol.* **2021**, *185*, 1411–1428.
- (14) Chen, J.; Nelson, D. C.; Shukla, D. Activation Mechanism of Strigolactone Receptors and Its Impact on Ligand Selectivity between Host and Parasitic Plants. J. Chem. Inf. Model. 2022, 62, 1712–1722.
- (15) Chen, J.; Shukla, D. Effect of histidine covalent modification on strigolactone receptor activation and selectivity. *Biophys. J.* **2023**, *122*, 1219–1228.
- (16) Gumbart, J. C.; Roux, B.; Chipot, C. Standard Binding Free Energies from Computer Simulations: What Is the Best Strategy? *J. Chem. Theory Comput.* **2013**, *9*, 794–802.
- (17) Gumbart, J. C.; Roux, B.; Chipot, C. Efficient Determination of Protein-Protein Standard Binding Free Energies from First Principles. J. Chem. Theory Comput. 2013, 9, 3789-3798.
- (18) Kästner, J. Umbrella sampling. Wiley Interdiscip. Rev.: Comput. Mol. Sci. 2011, 1, 932–942.
- (19) Kumar, S.; Rosenberg, J. M.; Bouzida, D.; Swendsen, R. H.; Kollman, P. A. THE weighted histogram analysis method for free-energy calculations on biomolecules. I. The method. *J. Comput. Chem.* **1992**, *13*, 1011–1021.

- (20) Shirts, M. R.; Chodera, J. D. Statistically optimal analysis of samples from multiple equilibrium states. *J. Chem. Phys.* **2008**, *129*, 124105.
- (21) Moffett, A. S.; Shukla, D. How do brassinosteroids activate their receptors? *BioRxiv* **2019**.
- (22) Zhao, C.; Shukla, D. Molecular basis of the activation and dissociation of dimeric PYL2 receptor in abscisic acid signaling. *Phys. Chem. Chem. Phys.* **2022**, 24, 724–734.
- (23) Serçinoğlu, O.; Ozbek, P. gRINN: a tool for calculation of residue interaction energies and protein energy network analysis of molecular dynamics simulations. *Nucleic Acids Res.* **2018**, *46*, W554–W562.
- (24) Chothia, C.; Janin, J. Principles of protein—protein recognition. *Nature* **1975**, 256, 705—708.
- (25) Tsai, C.-J.; Nussinov, R. Hydrophobic folding units at protein protein interfaces: Implications to protein folding and to protein protein association. *Protein Sci.* **1997**, *6*, 1426–1437.
- (26) Sundberg, E. J.; Urrutia, M.; Braden, B. C.; Isern, J.; Tsuchiya, D.; Fields, B. A.; Malchiodi, E. L.; Tormo, J.; Schwarz, F. P.; Mariuzza, R. A. Estimation of the Hydrophobic Effect in an Antigen-Antibody Protein-Protein Interface. *Biochemistry* **2000**, *39*, 15375–15387.
- (27) Keskin, O.; Gursoy, A.; Ma, B.; Nussinov, R. Principles of Protein-Protein Interactions: What are the Preferred Ways For Proteins To Interact? *Chem. Rev.* **2008**, *108*, 1225–1244.
- (28) Goh, C.-S.; Milburn, D.; Gerstein, M. Conformational changes associated with protein—protein interactions. *Curr. Opin. Struct. Biol.* **2004**, *14*, 104–109.
- (29) Wang, Q.; Zhang, P.; Hoffman, L.; Tripathi, S.; Homouz, D.; Liu, Y.; Waxham, M. N.; Cheung, M. S. Protein recognition and selection through conformational and mutually induced fit. *Proc. Natl. Acad. Sci. U.S.A.* **2013**, *110*, 20545–20550.
- (30) Gianni, S.; Dogan, J.; Jemth, P. Distinguishing induced fit from conformational selection. *Biophys. Chem.* **2014**, *189*, 33–39.
- (31) Chen, J.; White, A.; Nelson, D. C.; Shukla, D. Role of substrate recognition in modulating strigolactone receptor selectivity in witchweed. *J. Biol. Chem.* **2021**, 297, 101092.
- (32) Arellano-Saab, A.; Bunsick, M.; Al Galib, H.; Zhao, W.; Schuetz, S.; Bradley, J. M.; Xu, Z.; Adityani, C.; Subha, A.; McKay, H.; et al. Three mutations repurpose a plant karrikin receptor to a strigolactone receptor. *Proc. Natl. Acad. Sci. U.S.A.* **2021**, *118*, No. e2103175118.
- (33) Uraguchi, D.; Kuwata, K.; Hijikata, Y.; Yamaguchi, R.; Imaizumi, H.; Am, S.; Rakers, C.; Mori, N.; Akiyama, K.; Irle, S.; McCourt, P.; Kinoshita, T.; Ooi, T.; Tsuchiya, Y. A femtomolar-range suicide germination stimulant for the parasitic plant Striga hermonthica. *Science* **2018**, *362*, 1301–1305.
- (34) Pang, Z.; Zhang, X.; Ma, F.; Liu, J.; Zhang, H.; Wang, J.; Wen, X.; Xi, Z. Comparative Studies of Potential Binding Pocket Residues Reveal the Molecular Basis of ShHTL Receptors in the Perception of GR24 in Striga. *J. Agric. Food Chem.* **2020**, *68*, 12729–12737.
- (35) Shahul Hameed, U.; Haider, I.; Jamil, M.; Kountche, B. A.; Guo, X.; Zarban, R. A.; Kim, D.; Al-Babili, S.; Arold, S. T. Structural basis for specific inhibition of the highly sensitive ShHTL7 receptor. *EMBO Rep.* **2018**, *19*, No. e45619.
- (36) Nakamura, H.; Hirabayashi, K.; Miyakawa, T.; Kikuzato, K.; Hu, W.; Xu, Y.; Jiang, K.; Takahashi, I.; Niiyama, R.; Dohmae, N.; Tanokura, M.; Asami, T. Triazole Ureas Covalently Bind to Strigolactone Receptor and Antagonize Strigolactone Responses. *Mol. Plant* **2019**, *12*, 44–58.
- (37) Samejima, H.; Babiker, A. G.; Takikawa, H.; Sasaki, M.; Sugimoto, Y. Practicality of the suicidal germination approach for controllingStriga hermonthica. *Pest Manage. Sci.* **2016**, 72, 2035—2042.
- (38) Toh, S.; Holbrook-Smith, D.; Stokes, M. E.; Tsuchiya, Y.; McCourt, P. Detection of Parasitic Plant Suicide Germination Compounds Using a High-Throughput Arabidopsis HTL/KAI2 Strigolactone Perception System. *Chem. Biol.* **2014**, *21*, 988–998.

- (39) Arkin, M. R.; Wells, J. A. Small-molecule inhibitors of protein—protein interactions: progressing towards the dream. *Nat. Rev. Drug Discovery* **2004**, *3*, 301–317.
- (40) Ran, X.; Gestwicki, J. E. Inhibitors of protein-protein interactions (PPIs): an analysis of scaffold choices and buried surface area. *Curr. Opin. Chem. Biol.* **2018**, *44*, 75–86.
- (41) Sali, A.; Blundell, T. L. Comparative Protein Modelling by Satisfaction of Spatial Restraints. *J. Mol. Biol.* **1993**, 234, 779–815.
- (42) Fiser, A.; Do, R. K. G.; Šali, A. Modeling of loops in protein structures. *Protein Sci.* **2000**, *9*, 1753–1773.
- (43) Fiser, A.; Sali, A. ModLoop: automated modeling of loops in protein structures. *Bioinformatics* **2003**, *19*, 2500–2501.
- (44) Davidchack, R. L.; Handel, R.; Tretyakov, M. V. Langevin thermostat for rigid body dynamics. J. Chem. Phys. 2009, 130, 234101.
- (45) Feller, S. E.; Zhang, Y.; Pastor, R. W.; Brooks, B. R. Constant pressure molecular dynamics simulation: The Langevin piston method. *J. Chem. Phys.* **1995**, *103*, 4613–4621.
- (46) Darden, T.; York, D.; Pedersen, L. Particle mesh Ewald: An *N*-log(*N*) method for Ewald sums in large systems. *J. Chem. Phys.* **1993**, 98, 10089–10092.
- (47) Phillips, J. C.; Braun, R.; Wang, W.; Gumbart, J.; Tajkhorshid, E.; Villa, E.; Chipot, C.; Skeel, R. D.; Kalé, L.; Schulten, K. Scalable molecular dynamics with NAMD. *J. Comput. Chem.* **2005**, *26*, 1781–1802.
- (48) Minoukadeh, K.; Chipot, C.; Lelièvre, T. Potential of Mean Force Calculations: A Multiple-Walker Adaptive Biasing Force Approach. *J. Chem. Theory Comput.* **2010**, *6*, 1008–1017.
- (49) Comer, J.; Gumbart, J. C.; Hénin, J.; Lelièvre, T.; Pohorille, A.; Chipot, C. The Adaptive Biasing Force Method: Everything You Always Wanted To Know but Were Afraid To Ask. *J. Phys. Chem. B* **2015**, *119*, 1129–1151.
- (50) Roe, D. R.; Cheatham, T. E. PTRAJ and CPPTRAJ: Software for Processing and Analysis of Molecular Dynamics Trajectory Data. *J. Chem. Theory Comput.* **2013**, *9*, 3084–3095.



CAS BIOFINDER DISCOVERY PLATFORM™

# STOP DIGGING THROUGH DATA —START MAKING DISCOVERIES

CAS BioFinder helps you find the right biological insights in seconds

Start your search

